Geologia Croatica	68/3	285–302	8 Figs.	4 Tabs.		Zagreb 2015

Fluid inclusion study of the Boccassuolo VMS-related stockwork deposit (Northern Apennine ophiolites, Italy)

Gabriella B. Kiss

Department of Mineralogy, Eötvös Loránd University, 1/c Pázmány Péter sétány, Budapest, Hungary, H-1117; (gabriella.b.kiss@ttk.elte.hu)

doi: 104154/gc.2015.22

Geologia Croatica

ABSTRACT

Several Cyprus-type volcanogenic massive sulphide (VMS) deposits occur in the Jurassic ophiolitic series of the Northern Apennines. Stratabound, stratiform and stockwork deposits were formed in the western limb of the Neotethys (Ligurian Ocean) and are observed today in basalt, gabbro and serpentinised peridotite host rocks. The studied stockwork deposit at Boccassuolo occurs in basalt and basalt breccia. Detailed petrography, fluid inclusion study, Raman spectroscopy analyses and chlorite thermometry calculations were used to determine the P, T, X conditions of the fluid circulation system. The veins contain three quartz generations, calcite, chlorite, epidote and sericite as gangue minerals and pyrite, chalcopyrite, sphalerite, pyrrhotite and galena as ore minerals. Based on the fluid inclusion study, the earlier defined three vein types (1, 2 and 3) precipitated from the same type of evolving fluid, though at slightly different stratigraphic positions. The determined ranges of temperature (370-60°C), salinity (6.2-11.4 NaCl equiv. wt%), pressure (30-44 MPa) and methane content (average 0.28 mol/kg) suggest an evolved seawater origin for the hydrothermal fluid, modified by fluid-rock interactions and possibly by mixing of magmatic volatiles. The fluid characteristics and the mineralogical observations have proven a slightly distal position in relation to the centre of the fluid flow for all the studied locations, but more central and more distant blocks were also recognised. The temporal evolution of the system developed into a low temperature event, occurring after the main mineral stage of formation, but still within the same overall process.

Keywords: hydrothermal processes, VMS deposit, ophiolite, Northern-Apennines, fluid inclusions, Raman spectroscopy

1. INTRODUCTION

Numerous volcanogenic massive sulphide (VMS) deposits with a Cyprus-type metallogenic signature (Cu-Fe-Zn) occur in the Tethyan Jurassic ophiolites (the Ligurides) of the Italian Northern Apennines. One of these deposits, Boccassuolo, is located close to the city of Modena. It consists of sulphide mineralisation in quartz veins which cut across pillow-basalt and basalt breccia. This stockwork mineralisation consists of pyrite, chalcopyrite, and sphalerite, with (in the upper levels), galena, occurring together with quartz, calcite and chlorite (see e.g. GARUTI et al., 2008, 2011 and the references therein). On the basis of the Pb-Ag-Au-Zn-Cu distribution pattern, GARUTI et al. (2011) recognised three major types of mineralised veins.

Historical mining activity at Boccassuolo enables research at several levels of the stockwork mineralisation. This convenient situation allows modelling the vertical and horizontal features of the mineralised hydrothermal system. In spite of this, only an attempt to evaluate the temperature of the mineralised fluids in Boccassuolo was done by using a chlorite geothermometer (ZACCARINI & GARUTI, 2008), but a detailed description of the characteristics of the hydrothermal fluids is not currently available. The present study describes this phenomenon more precisely, with the help of detailed fluid inclusion microthermometry, Raman spectroscopy and chlorite thermometry studies in all three types of Boccassuolo veins. Characteristics of the P, T, X conditions of the hydrothermal fluid helps to link genetically the three vein-types and allows a model of the fluid circulation system to be established. It could serve also as a base for future work in the other Ligurian VMS deposits. Furthermore, comparison of the temperature obtained using fluid inclusion microthermometry with those calculated with a chlorite geothermometer allows us to evaluate the research efficiency of this latter approach.

2. REGIONAL GEOLOGY AND DESCRIPTION OF THE VMS DEPOSITS

The small mass of ophiolite of Boccassuolo pertains to the Ligurian Ophiolite Belt (Fig. 1A) extending from the Western Alps to the Northern Apennines and northeastern Corsica (GARUTI et al., 2008, 2011, and references therein). The Ligurian Ophiolites formed in the westernmost limb of the Neotethys by rifting of the Adria and European continental plates. They are considered as typical examples of subduction-unrelated, continental margin ophiolites (BARRETT, 1982; PICCARDO et al., 2002; DILEK & FURNES, 2011, 2014).

Asymmetric extension induced by a detachment fault initially caused the subcontinental mantle to be intruded by small gabbroic plutons and mafic dykes (from the Triassic to the Middle Jurassic). As a consequence of continental breakup, the peridotite-gabbro basement was exposed and deeply eroded at the floor of the incipient ocean (the Piedmont-Liguria Basin). Extensive formation of thick horizons of ophicalcite and serpentinite-gabbro breccia marked these initial episodes of seafloor erosion (CORTESOGNO et al., 1978, PRINCIPI et al., 1992). Further ocean opening occurred in a slow-spreading regime producing scattered and limited extrusion of MORB-type lava lying directly on the plutonic rocks (BARRETT, 1982; LEMOINE et al., 1987; LAGABRIELLE & LEMOINE, 1997; PICCARDO et al., 2002).

The upwelling mafic magma provided the heat for the establishment of convective hydrothermal cells across the Ligurian sub-oceanic crust and led to the consequent formation of VMS-type Cu-sulphide deposits, characterised by their different ore composition and sulphur isotope signature

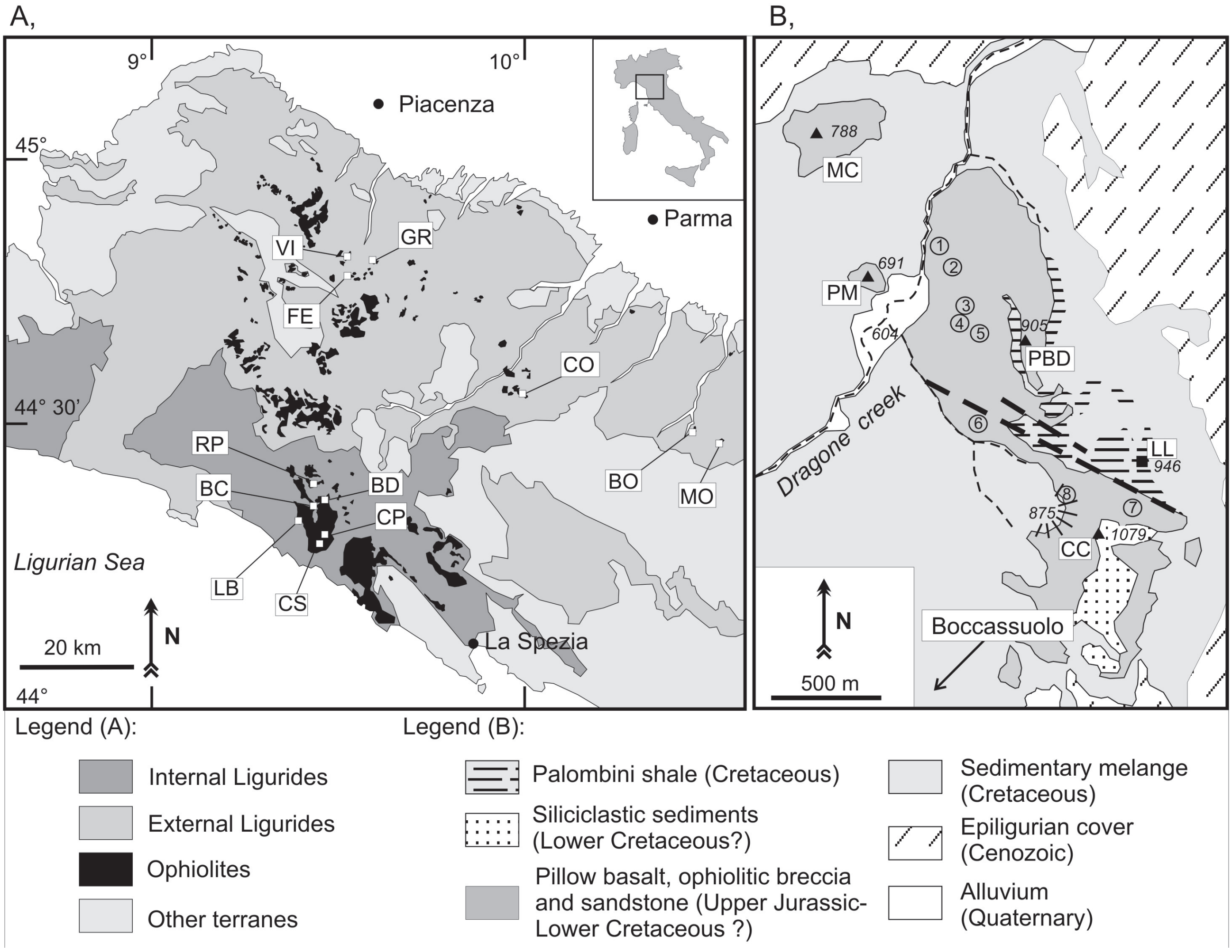

Figure 1: Structural sketch of the ophiolites of the Northern Apennines (**A**) and a simplified geological map of the Boccassuolo ophiolite (**B**) (GARUTI et al. 2011). The location of Figure 1B is marked with the sign BO on Figure 1A. Figure 1B shows the sampling sites (numbers 1-8 in circles) and the elevations (italic numbers, in metres) above sea level. The ophiolite locations discussed in the text are: BC-Monte Bianco, BD-Monte Bardeneto, BO-Boccassuolo, CO-Corchia, CP-Campegli, CS-Casali, FE-Ferriere, GR-Groppallo, LB-Libiola, MO-Montecreto, RP-Reppia, VI-Vigonzano. The parts of the Boccassuolo ophiolite are: CC-Cinghio del Corvo, LL-Cascina Lame, MC-Madonna del Calvario, PBD-Poggio Bianco Dragone, PM-Poggio Medola.

according to their distinctive structural position in the ophiolite stratigraphy (FERRARIO & GARUTI, 1980; GARUTI & ZACCARINI, 2005; GARUTI et al., 2008, 2009). Hydrothermal activity, preceding the outflow of basaltic lava, generated deposition of sulphides in stockwork-veins crosscutting the peridotite-gabbro basement (at Vigonzano, Ferriere, Groppallo, Santa Maria and Campegli), and in the formation of stratiform ore bodies within the seafloor serpentinite breccia (at Monte Bardeneto, Reppia and Monte Bianco). The seafloor-stratiform deposits are invariably covered with pillow lava flows, whereas no significant deposition of sulphide was observed in the serpentinite breccia overlain by sediments. This observation supports the conclusion that formation of hydrothermal cells and subsequent discharge of metals on the seafloor were essentially focused around centres of uprising magma, during a relatively long volcanic hiatus preceding the basalt extrusion (GARUTI et al., 2008). The hydrothermal activity continued during and after basalt outflow, thereby sulphides were deposited in crosscutting stockwork-veins (at Casali, Reppia, Monte Bianco, Montecreto and Boccassuolo) and conformable ore bodies within the basalt unit, as well as in seafloor-stratiform ore bodies on top of the volcanic pile (at Reppia, Corchia and Libiola) (Fig. 1A) (ZACCARINI & GARUTI, 2008).

The overlying rocks of the VMS-bearing oceanic units are pelagic sediments. Firstly radiolarian chert (Upper Jurassic) was deposited, accompanied by intensive exhalative hydrothermal activity leading to the formation of huge manganese deposits (BONATTI et al., 1976; CABELLA et al., 1998). Progressive regression of the oceanic crust from the axial rifting zone was marked by burial of the ophiolitic basement under a thick cover of pelagic sediments, mainly represented by Calpionella Limestone and Palombini Shale (Lower- to Upper-Cretaceous), overlain by various types of arenaceous turbidites (Upper-Cretaceous to Palaeocene). Palombini Shale may occur also as a sedimentary intercalation within the pillow basalt (e.g. at Boccassuolo) and can be found as a component of „debris-flow-type" polygenic breccia (together with chert, basalt, serpentinite and rare granite), indicating that continuing episodes of seafloor erosion occurred at intervals coeval with basaltic volcanism and pelagic sedimentation. This geotectonic evolution resulted in the build-up of the anomalous architecture of the Ligurian Ophiolites, consisting of weakly depleted subcontinental mantle, directly overlain by a volcano-sedimentary cover with thick accumulations of ophiolitic breccia, but lacking a true, mafic-ultramafic cumulus pile and sheeted-dyke complex, which are typical members of the conventional ophiolite stratigraphy (BARRETT & SPOONER, 1977; ABBATE et al., 1980; BARRETT, 1982; CORTESOGNO et al., 1987; LEMOINE et al., 1987; PRINCIPI et al., 1992; PICCARDO et al., 2002).

Convergence across the Piedmont-Liguria Basin (Upper-Cretaceous to Eocene) resulted in subduction of the western limb of the oceanic crust beneath the Adria continental margin. The subducted oceanic lithosphere and associated sulphide deposits underwent eclogite-facies metamorphism and during the Alpine orogeny, were obducted along the Western Alps and the Western Liguria Apennines (Dal PIAZ, 1974 a,b; POGNANTE & PICCARDO, 1984; LOMBARDO et al., 2002). In contrast, large fragments of oceanic lithosphere preserved from the high-P, low-T metamorphism, are presently exposed in the Northern Apennines, between eastern Liguria and southwest Emilia Romagna and partly in northeastern Corsica. These ophiolites and related sulphide deposits of the Northern Apennines show the effects of sub-oceanic hydrothermal metasomatism (BARRETT & FREIDRICHSEN, 1989), or weak metamorphism to the lower limit of the prehnite-pumpellyite facies and orogenic deformation in a cold regime (CORTESOGNO et al. 1975). Mineralogy of shale from the sedimentary cover reflects P-T conditions compatible with extreme burial diagenesis (LEONI et al., 1998; ZACCARINI & GARUTI, 2008). These ophiolites form a composite nappe in which fragments of oceanic crust proximal to the axial rifting zone (Internal Ligurides) are thrust northeastward over ophiolites and sediments exhumed from more distal zones, close to the Adria continental margin (External Ligurides). The Internal Ligurides consist of NE-verging blocks bounded by southwestward dipping faults, in which stratigraphic contact between ophiolites and sedimentary cover is commonly preserved (ELTER, 1975; BARRETT, 1982). The External Ligurides are characterised by dismembered ophiolitic blocks of kilometre to metre size, embedded in a mélange formed by polyphase tectonic disruption of the Cretaceous sedimentary cover (Fig. 1A) (PINI, 1999). Due to the intense tectonism, stratigraphic relationships among ophiolite units are preserved only inside the largest ophiolite blocks (GARUTI et al., 2008).

3. THE GEOLOGY OF THE BOCCASSUOLO OPHIOLITE

The Boccassuolo ophiolite (Fig. 1B), preserved from the high P low T metamorphism, is located in the External Ligurides, at about 44° 18' N and 10° 37' E, southwest of the city of Modena (Emilia Romagna). The ophiolitic rocks form a N-S elongated body of about 4 x 1.5 km, composed of two major blocks: Poggio Bianco Dragone to the north and Cinghio del Corvo to the south, separated by a NW-SE trending subvertical fault (GARUTI et al., 2011). The ophiolite is made up of an alternation of lava flows (pillow and massive basalt) intercalated with several metre thick horizons of ophiolitic sediments (breccia and sandstone), composed of clasts of basalt, chert, limestone and rare serpentinite and granite. These ophiolitic rocks tectonically overlie strongly deformed carbonaceous-argillaceous sediments, poorly exposed at the northeastern border of the ophiolite. No mafic-ultramafic basement has been observed at Boccassuolo. Close to the top of the Cinghio del Corvo block (1079 m), pillow and pillow breccias are stratigraphically capped by siliciclastic sediments containing thin layers of Mn-rich clay (early pelagic sedimentation?), although, the original presence of a thick formation of chert in the sedimentary cover of the Boccassuolo ophiolite is supported by the occurrence of large blocks (up to several metres in size) of radiolarian chert within the ophiolitic breccia. The ophiolitic rocks of the Poggio Bianco Dragone block reach a maximum exposed thickness of about 350 m, with a general attitude varying from NW-dipping (~10° to 45° degrees) at the base, to nearly horizontal close to the top. The original thickness of the entire volcano-sedimentary pile is estimated to have not exceeded 500 m, from a possible ultramafic footwall to the overlying sedimentary cover (PLESI et al., 2002).

4. THE MINERALISATION OF THE BOCCASSUOLO VMS DEPOSIT

The sulphide deposit of Boccassuolo (Fig. 1B) consists of a reticulate stockwork of quartz-calcite-chlorite-sulphide veins emplaced in pillow basalt and ophiolitic breccia (ZACCARINI & GARUTI, 2008, GARUTI et al., 2011). The veins vary in thickness from 10 to 30 centimetres, but giant veins of 0.5 to 1.5 metres diameter have also been observed locally. The pillow basalt shows progressively increasing spilitic alteration from the outside towards the core of the stockwork pipe, with the appearance of disseminated pyrite (GARUTI et al., 2011). Individual veins cutting across pillow basalt may have weakly deformed, sharp contacts with the country rock, or display disrupted irregular boundaries generating an anastomosing texture in which centimetre to decimetre sized fragments of strongly spilitised basalt are engulfed. Veins cutting across the ophiolitic breccia have irregular, diffuse boundaries derived from permeability-controlled infiltration of fluids into the country rock. Here, the mineral corrensite ($(Mg,Fe)_9((Si,Al)_8O_{20})(OH)_{10} \cdot nH_2O$) has been identified as a major component of the clayey matrix of the breccia. The occurrence of corrensite possibly indicates the reaction of the original clay minerals with a hot hydrothermal solution (DAOUDI & POT de VIN, 2002). The ophiolitic sandstone is usually barren, or weakly mineralised with infiltration of minute calcite-epidote-sulphide fissure filling and impregnation. Epigenetic veins containing abundant datolite ($CaBSiO_4(OH)$) have also been described (GARUTI et al., 2008, 2011; ZACCARINI et al., 2008).

Relevant mining sites, prospects and outcrops predominate in the northern block of the Boccassuolo ophiolite (Fig. 1B). The veins form a sub-vertical pipe extending between 600 m, at the lower level of the Due Livelli mine (site nr. 1), up to the elevation of about 750 m, above the Labirintica mine (site nr. 5). Between these two localities, mineralised veins had been intercepted by mining works at the altitudes of 654 m (Lumaca prospect, site nr. 2), 663 m (Allagata mine, site nr. 3), and 673 m (Dolicopoda-Pipistrello prospects, site nr. 4). Furthermore, a single vein up to 1 m thick (Filone 101) is exposed between sites nr. 2 and 3 (GARUTI et al., 2011).

In the southern block, a few veins crop out in small mining prospects (trenches and galleries) close to the Lame locality (site nr. 7, 1031-1060 m) northeast of the Cinghio del Corvo peak (1079 m). Two previously unknown sulphide occurrences have been recently brought to light by natural erosion (Filone Omar, site nr. 6, 880 m), or dug out during quarrying work for basaltic aggregate (Cinghio del Corvo quarry, site nr. 8, 874 m). In both the northern and southern blocks, the stockwork mineralisation disappears upwards, apparently not tectonically interrupted, but topped by new pillow lava and basalt breccia debris flows (GARUTI et al., 2011).

Major sulphide minerals are pyrite (±accessory pyrrhotite), along with variable amounts of chalcopyrite, sphalerite and galena, minutely disseminated in a quartz-carbonate-chlorite gangue (BERTOLANI, 1953; ZACCARINI & GARUTI, 2008). Based on the Pb-Ag-Au-Zn-Cu distribution pattern, three major types of veins have been identified (GARUTI et al., 2011):

Type 1 is characterised by high Cu (2.09 – 5.94 wt%), Zn (1.92 – 4.85 wt%), Ag (2.9 – 7.28 ppm), Au (11-17 ppb), and Pb below the detection limit of 0.3 ppm.

Type 2 is the most common sulphide mineralisation, with variable concentrations of Cu (20 ppm – 3.89 wt%), Zn (0.01 – 2.31 wt%), Ag (2.0 – 13 ppm) and Au (2.0-13 ppb), but characterised by a moderate Pb content (3.43 – 117 ppm).

Type 3 is rare, and shows low Cu (0.02 – 0.6 wt%), Zn (0.01 – 0.44 wt%), Ag (0.63 – 1.08 ppm) and Au (4.1-6.5 ppb), but relatively high Pb (906 – 1532 ppb) which accounts for the abundant galena in the sulphide mineral assemblage.

The concentration of sulphide increases from a low-grade (1.06-2.09 wt% sulphur) to medium-grade (3.0-6.2 wt% sulphur) in type 2 and 3 veins and relatively high-grade (8.73-12.3 wt% sulphur) in type 1 and 2 veins. The appearance of distinctive Pb anomalies in the veins of Boccassuolo, compared with other stockwork vein deposits in the Northern Apennine ophiolites, has been interpreted as evidence of their emplacement in a transition zone from the Ligurian mid-oceanic-ridge to the Adria continental margin (GARUTI et al., 2011).

5. SAMPLING AND ANALYTICAL TECHNIQUES

A total of 104 samples were collected from abandoned galleries, dumps (in front of the galleries) and natural outcrops of 8 different levels (sites no. 1-8, see above) of the Boccassuolo ophiolite (Fig. 1B). Thirty-three representative samples of the sulphide mineralisation were selected for the fluid inclusion study (Table 1), in part they are the same samples analysed in previous works (ZACCARINI & GARUTI, 2008, GARUTI et al., 2009, 2011), in part they are samples studied in detail only during this investigation (therefore they were not classified into vein types by GARUTI et al. 2011).

Petrography of the studied samples was carried out with a Zeiss Axioplan microscope. The work was completed with observations in IR light, using a Hamatsu C2400 camera (spectral response from 400 nm to 1800 nm) system mounted on an Olympus BH2 type microscope. Fluid inclusion petrography and a microthermometric study were carried out on 80-100 μm thick, double polished sections of the stockwork veins, using a Linkam FT-IR 600 type heating freezing stage mounted on an Olympus BX-51 type polarizing microscope providing 1000x magnification. The precision of the microthermometric measurements was ±0.1 °C below 0 °C, and ±1 °C above it. The calibration of the instrument was made by analysis of CO_2 and pure water synthetic fluid

Table 1: List of the studied samples.

Site nr.	Mine	Vein type*	Sample nr.	Description	Mineral composition									
					Pyrite	Pyrrhotite	Chalcopyrite	Sphalerite	Galena	Quartz	Calcite	Chlorite	Sericite	Epidote
1		-	BO53	mineralised vein	X		X	X		X	X	X	X	
1	Miniera dei Due Livelli	-	BO55	mineralised vein	X		X	X		X	X		X	
1		-	BO56	poorly mineralised vein	X		X	X		X	X		X	
2-3	-	-	BO101	mineralised vein	X					X			X	
3	Galleria Allagata	-	BO42	mineralised vein	X		X	X		X			X	
3		-	BO78	mineralised vein	X		X	X		X			X	
4	Galleria Dolicopoda	-	BO9	mineralised vein	X		X	X		X	X	X	X	
4		type 2	BO38	mineralised vein	X		X	X		X	X	X	X	
4	-	type 1	BO33	mineralised vein	X	X	X	X		X	X	X	X	
4	Galleria del Pipistrello	type 2	BO28	mineralised vein	X		X	X		X	X	X	X	
4		-	BO65	mineralised vein	X		X	X		X	X	X	X	
5		-	BO1	mineralised vein	X		X	X		X	X	X	X	
5		-	BO2	mineralised vein	X	X	X	X		X	X		X	
5	Galleria Labirintica	type 1	BO3	mineralised vein	X		X	X		X	X	X	X	
5		type 1	BO5	mineralised vein	X		X	X		X	X	X	X	
5		type 1	BO6	mineralised vein	X		X	X		X		X	X	
6		-	BO95	banded vein in basalt breccia	X		X	X		X	X		X	
6		-	BO96	banded vein in basalt breccia	X		X	X		X	X		X	
6	Filone Omar	type 2	BO97	vein in basalt breccia	X		X	X		X	X	X	X	
6		type 2	BO98	vein in basalt breccia	X	X	X	X		X	X	X	X	
6		-	BO99	vein in basalt breccia	X		X	X		X	X		X	
6		-	BO100	vein in basalt breccia	X		X	X		X	X		X	
7	Le Lame	type 2	BO35	mineralised vein	X		X	X		X		X	X	
7		type 2	BO36	mineralised vein	X		X	X		X		X	X	
8		type 2	BO11	mineralised vein	X		X	X		X	X	X	X	
8		type 2	BO12	mineralised vein	X		X	X		X	X	X	X	
8		type 2	BO14	mineralised vein	X		X	X		X	X	X	X	
8		-	BO18	mineralised vein	X		X	X		X	X	X	X	X
8	Cava dei Cinghi	-	BO90	mineralised vein	X		X	X	X	X	X	X	X	
8		type 3	BO91	mineralised vein	X		X	X	X	X	X	X	X	
8		type 3	BO92	mineralised vein	X		X	X	X	X	X	X	X	
8		type 3	BO93	mineralised vein	X		X	X	X	X	X	X	X	
8		-	BO94	mineralised vein	X		X	X	X	X	X	X	X	
total number of samples: 33														

*: vein types according to GARUTI et al. 2011, applied only for samples, which were classified in that study.

inclusions. These analyses were carried out at the Eötvös Loránd University, Department of Mineralogy.

Raman microanalysis of fluid inclusions in quartz and calcite was completed at the Eötvös Loránd University, Faculty of Science, Research Instrument Core Facility, using a Horiba Yvon Jobin LabRAM HR 800 edge filter based confocal dispersive Raman spectrometer, 800 mm focal length, coupled with an Olympus BXFM type microscope. During the measurements, 532 nm emission of a frequency doubled Nd:YAG laser, 600 grooves/mm grating, 50 μm confocal aperture and 50x and 100x long working distance objective were used. For some measurements, the Linkam FTIR 600 microthermometric stage was mounted to the spectrometer and analyses were performed at different temperatures from -50 °C to +355°C.

Interpretation of the microthermometric and Raman spectroscopic data was carried out using the methods of GUILLAUME et al. (2003), DUAN & MAO (2006) and SUN et al. (2010) and using PeakFit v. 4.12. software by Seasolve Software Inc. For salinity calculations (SUN et al., 2010), the same treatment was performed in each case: the baselines were corrected by the linear method, the spectra were fitted with two Gaussian functions (fitting parameter R^2=0.995-0.997). The effects of measurement conditions and data fitting procedure were eliminated by calculating the difference between the solution and pure water. As the base of the calculations is the good quality Raman spectra of the aqueous liquid phase of the inclusions, only those are applied in the study, which are characterised by >10μm size, stationary gas bubble and are occurring deep in the samples.

Chlorite thermometry calculations are based on the chlorite composition database of ZACCARINI & GARUTI (2008), and new electron microprobe analyses performed at the Eugen Stumpfl Microprobe Laboratory (University of Leoben) using a Jeol Superprobe JXA-8200, operated at 15 kV accelerating voltage, 10 nA beam current, ~1 μm beam diameter, and counting times of 20 and 10 seconds for peak and backgrounds, respectively. The X-ray Kα lines for Si, Mg, Al, Ti, Cr, Ca, Na, K, Mn, Fe, and natural silicates and chromium spinel as standards were used for the analysis of chlorite. The method of CHATELINEAU & IZQUIERDO (1988) with an uncertainty of about 20°C was used to calculate the formation temperature of the chlorite, as the measured Al(IV) and XFe amounts of the individual crystals fitted into the criteria of that method.

6. CHARACTERISATION OF THE HYDROTHERMAL PROCESSES

6.1. Petrography of the veins

The studied veins occur in strongly altered basalt. The original variolitic texture of the basalt is hardly traceable; the rock is almost completely altered to clay minerals, chlorite and fine grained quartz. It is commonly cross-cut by <1 mm thick quartz veins. The basalt-vein contact is sharp and contains –besides a few altered glassy basalt clasts– the same minerals, as the other parts of the vein.

The studied veins were partly classified by GARUTI et al. (2011) into vein types 1, 2, and 3, but samples without this earlier classification were also studied (Table 1). However, based on the available results (GARUTI et al., 2011), the northern block of the Boccassuolo ophiolite (sites nr. 1-5) contains only types 1 and 2, while the southern block (sites nr. 6-8) contains only types 2 and 3 veins. According to the observations, no significant difference in the occurring gangue and ore minerals was observed between vein types 1, 2 and the unclassified samples, although the amounts of the ore minerals may vary. In contrast, vein type 3 differs notably, since galena occurs only in these veins. Based on these, a summarising description is presented here, and the occurrence of the different gangue and ore minerals at the various localities is shown in Table 1.

Quartz is the most common gangue mineral found in the veins. Generally, it occurs in all 3 vein types in 3 generations, corresponding to the sequence of crystallisation events (Fig. 2A); quartz 1 is the oldest, while quartz 3 is the youngest. Quartz 1 (Qtz1) is characterised by 1-10 mm euhedral and subhedral, commonly growth zoned crystals with a spongy core. They frequently show a comb structure resulting from open-space filling from the vein walls inward. Quartz 2 (Qtz2) is typically 0.1-1 mm subhedral, barely transparent quartz, while quartz 3 (Qtz3) is commonly <0.05 mm in size and forms anhedral crystals. Qtz3 may form thin veinlets, with/without carbonate and sulphides, cross-cutting or sometimes even brecciating the earlier quartz grains (Fig. 2B). In general, all three generations are observed at every locality, though their relative amounts may be different. The only exception is site nr. 6, where only Qtz2 and Qtz3 were observed.

Sericite occurs commonly as <10 μm sized anhedral grains among the quartz crystals and also as solid inclusions within them. Carbonate and chlorite consist of 0.1-1 mm sized anhedral grains (Fig. 2A, C, D), occurring rarely cogenetically with, most commonly epigenetically to the quartz crystals.

Sulphide minerals occur disseminated interstitially or as solid inclusions in both quartz generations, usually showing a banded distribution, symmetrical around the centre of the vein. Therefore, early and late sulphides were also distinguished. Except for samples from sites nr. 2-3, where only pyrite occurs, pyrite is commonly accompanied by chalcopyrite, sphalerite and rarely galena and pyrrhotite, forming up to 5-50 area% of the ore.

The pyrite may form eu-, sub- and anhedral crystals up to 5 mm in size, and can be one of the most common ore minerals (Fig. 2E, F). None of the crystals are transparent in IR light. Chalcopyrite is the second most common ore mineral, varying between 5-50 area% of the ore. It forms up to 1 mm sized anhedral crystals (Fig. 2F, G). Sphalerite occurs at almost each studied locality, forming anhedral grains up to 2 mm in size. Its amount varies between 1-10 area% of the ore. Grains with signs of „chalcopyrite disease" are common (Fig. 2E, H), though some crystals are lacking this feature. The formers are not transparent in IR light, while the

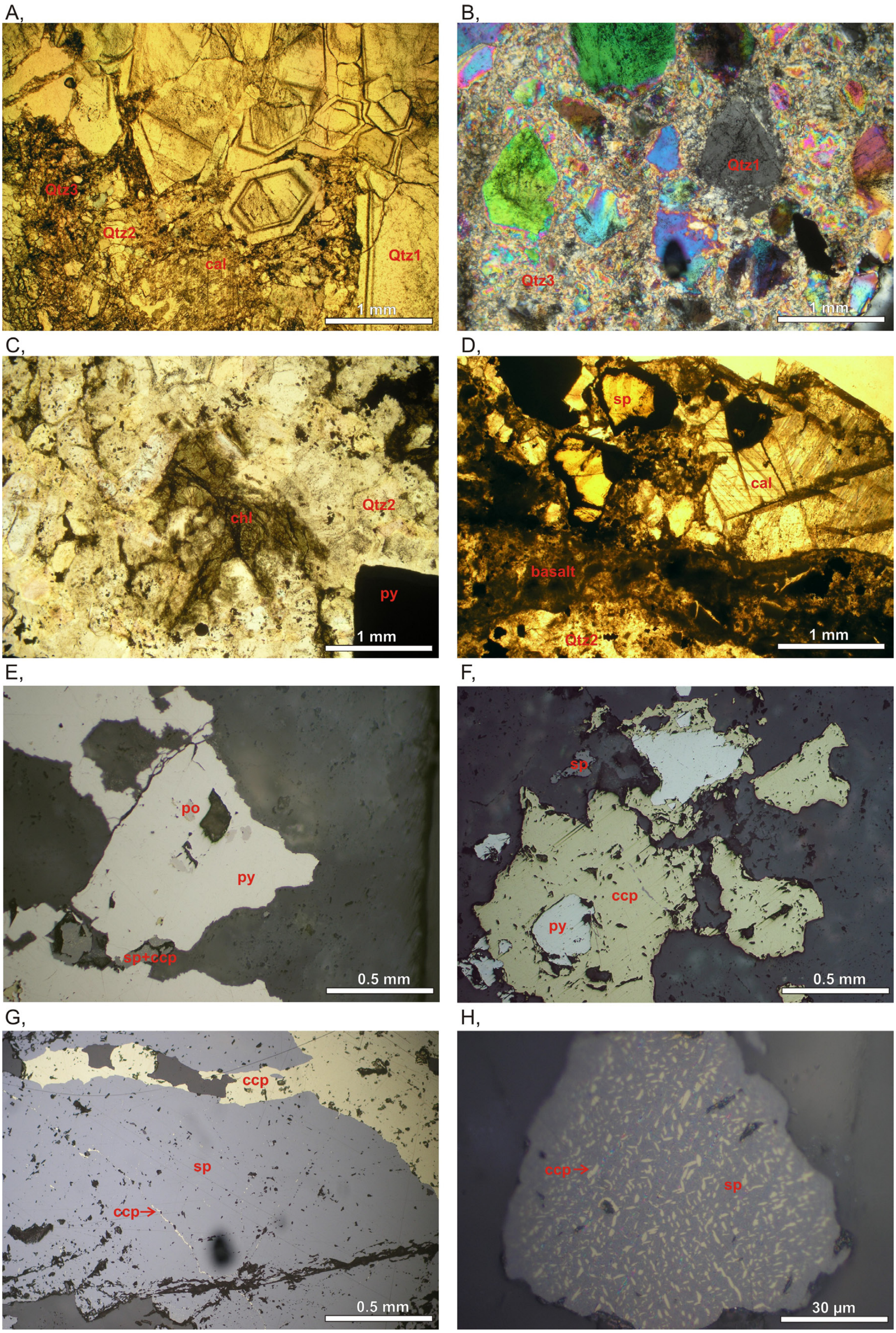

Figure 2: Typical textures of the gangue and ore minerals under polarizing microscope. **A:** Euhedral and subhedral coarse grained Qtz1, the remaining space is filled by Qtz2, Qtz3 and calcite (cal) (site nr. 8, 1N). **B:** The coarse grained Qtz1 is brecciated by Qtz3 (site nr. 2-3, +N). **C:** Chlorite (chl) fills up the space among the crystals of Qtz2 (site nr. 3, 1N). **D:** Strongly altered basalt with Qtz2, transparent sphalerite (sp) and late calcite (site nr. 6, 1N) **E:** Pyrrhotite (po) inclusions in early pyrite (py), and later sphalerite (sp) with chalcopyrite (ccp) disease (site nr. 4, 1N). **F:** Chalcopyrite consuming the early pyrite (site nr. 4, 1N). **G:** Later chalcopyrite veins cutting the earlier sphalerite (site nr. 6, 1N). **H:** Chalcopyrite disease in sphalerite (site nr. 4, 1N).

latter ones are transparent even in VIS (Fig. 2D). Pyrrhotite occurs only as <0.05 mm inclusions within the pyrite (Fig. 2E). The amount of this mineral is always <1 area% of the ore. Galena forms anhedral grains up to 0.3 mm, forming up to 5-10 area% of the ore in the type 3 veins of site nr. 8.

Based on the textural features, a generalised mineral precipitation sequence is postulated (Fig. 3).

6.2. Fluid inclusion petrography

Fluid inclusions were observed at all sites (nr. 1-8), vein types (1-3) and quartz generations (Qtz1, Qtz2 and Qtz3), in both the calcite and sphalerite. As no significant petrographic difference was observed among the fluid inclusions of vein types 1- 3, or between the different sites, a summary description is presented here. All the studied minerals were barely transparent, due to the extremely high amount of secondary fluid inclusion planes, which created difficulties during the petrographic study.

Qtz1 and Qtz2 contain rare, generally 4-7 μm sized, rectangular shaped, two-phase (liquid, L and vapour, V) fluid inclusions of primary origin, either in the growth zones or in the spongy core of the crystals (Fig. 4A, C). The phase ratio is fairly constant (10-20 area% V and 90-80 area% L), suggesting a homogenous entrapment from a homogenous parent fluid. The inclusions rarely reach 15-20 μm in size and/or contain accidentally trapped, irregularly shaped solid phase(s) (S) (Fig. 4D). Identification of the primary inclusions was hindered by the high amount of secondary inclusions, of which several generations were observed. One of these is characterised by similar features, like the primary inclusions of Qtz3, while other generations of single-phase (L) and two-phase (L+V, V <5 area%), 1-25 μm sized inclusions with irregular or rounded shape also occur.

Qtz3 contains rarely 4-20 μm sized, rectangularly shaped, single- (L) or two-phase (L+V) fluid inclusions of primary origin, occurring far from the secondary planes (Fig. 4E). The phase ratio is fairly constant (5-10 area% V and 95-90 area% L) in the two-phase inclusions, suggesting a homogenous entrapment from a homogenous parent fluid.

The calcite contains rarely 4-20 μm sized, negative crystal shaped, single- (L) or two-phase (L+V) fluid inclusions of primary origin, occurring far from the secondary planes (Fig. 4B). The phase ratio is fairly constant (5-10 area% V and 95-90 area% L) in the two-phase inclusions, suggesting a homogenous entrapment from a homogenous parent fluid. Extremely high numbers amounts of secondary planes occur, containing commonly one-phase (L) inclusions, but two-phase (L+V, V<5 area%) inclusions are also observed.

The one-phase (L) primary inclusions of Qtz3 and the calcite may be interpreted as a phenomenon of metastable stretched liquid. This inhibits the formation of a vapour bubble during cooling and hence precludes measurement of Th at T below ~65 °C (GOLDSTEIN & REYNOLDS, 1994; DIAMOND, 2003).

The sphalerite is rich in secondary planes (Fig. 4H), containing one-phase (L), rarely two-phase (L+V, V~5 area%), rectangularly shaped inclusions of 5-20 μm in size. In the growth zones of the crystals, solid chalcopyrite inclusions (Fig. 4F, G), together with some poorly observable (due to their small size and dark outline) fluid inclusions occur. Far from the secondary planes, 10-20 μm sized, rectangular shaped, two-phase (L + V) primary inclusions are rarely observed (Fig. 4I), with a constant phase ratio (~20 area% V and ~80 area% L). Despite of its scarce occurrence, based on the textural similarities with the inclusions of Qtz1 and Qtz2, a homogenous entrapment from a homogenous parent fluid is assumed.

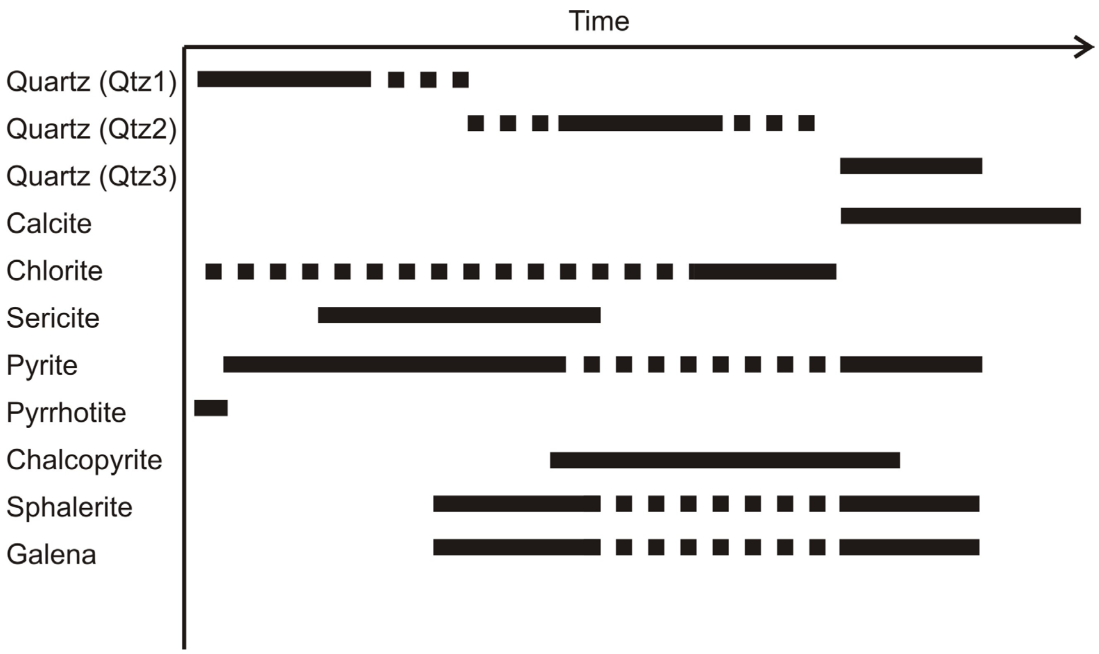

Figure 3: The temporal series of mineral precipitation in the studied stockwork veins.

6.3. Microthermometric study

Fluid inclusion microthermometry was carried out on the different quartz generations, as well as on calcite grains. The results were evaluated according to the different sites as well as the vein types, in order to be able to draw more precise conclusions. Analyses were carried out on well defined fluid inclusion assemblages, only where the petrographic association of the inclusions was unambiguous and they represented the original trapped fluid. Measurements on Qtz3 were often

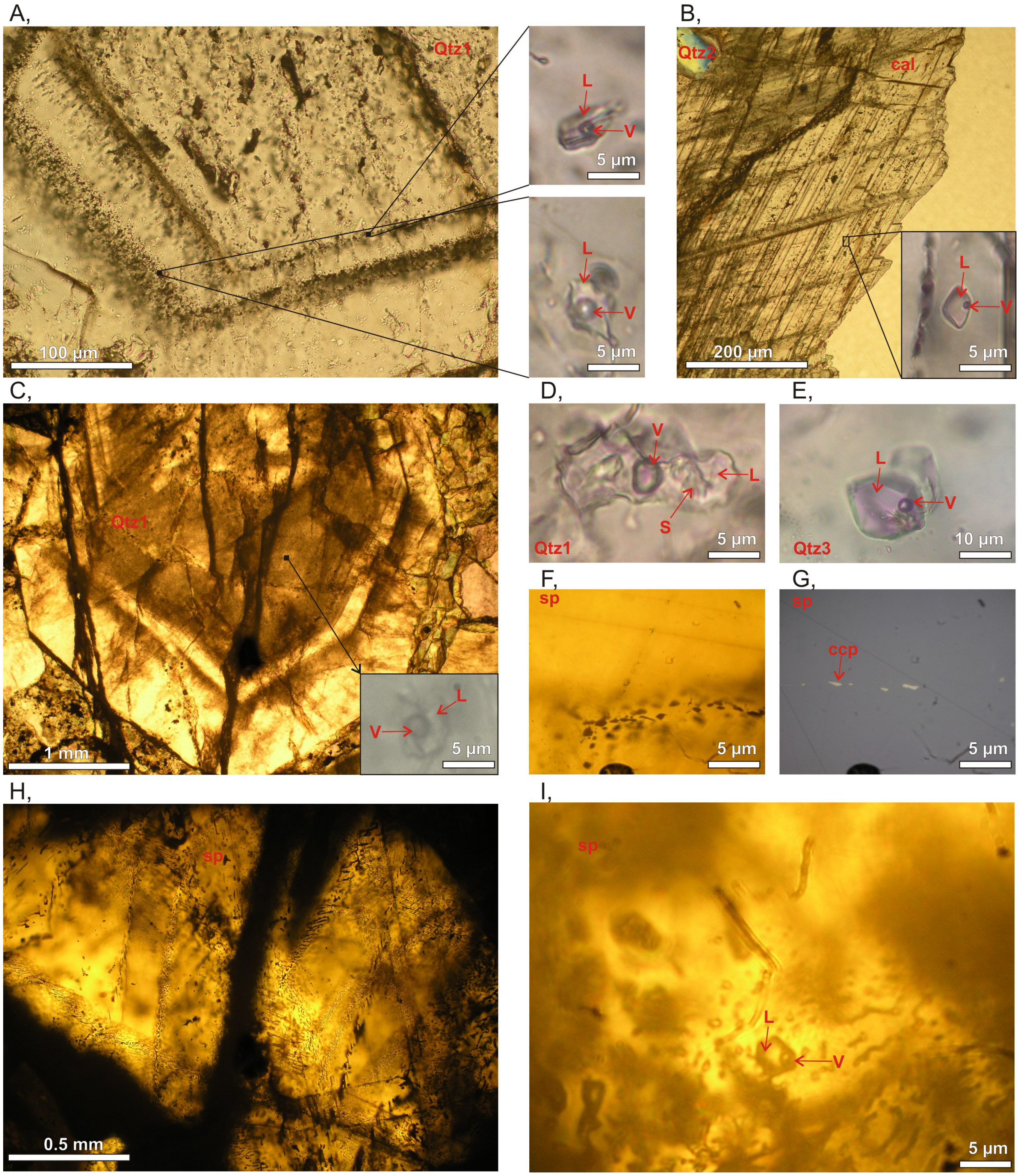

Figure 4: Typical textural features of the fluid inclusions in quartz, calcite and sphalerite. **A:** Two-phase L+V primary fluid inclusions in the growth zones of Qtz1 (site nr. 8). **B:** Two-phase L+V primary fluid inclusions among the secondary planes of the late calcite (site nr. 8). **C:** Two-phase L+V primary fluid inclusion in the spongy core of Qtz1 (site nr. 5). **D:** Three-phase L+V+S, accidentally trapped mineral containing fluid inclusion in Qtz1 (site nr. 2-3). **E:** Two-phase L+V primary fluid inclusion in Qtz3 (site nr. 1). **F:** Chalcopyrite inclusions in the growth zone of sphalerite (site nr. 6). **G:** the same location under a reflected light microscope (site nr. 6, 1N). **H:** Abundant secondary inclusion planes in transparent sphalerite (site nr. 6). **I:** Two-phase L+V primary fluid inclusion in sphalerite (site nr. 6).

Table 2: Fluid inclusion microthermometry studies in quartz and calcite and chlorite thermometry calculations.

Site nr.	Vein type*	Mineral	Number of measurements	Average Th (LV-L) (°C)	St.dev. Th (°C)	Average Tm (cla) (°C)	St. dev. Tm (cla) (°C)	Average formation T (°C)	St.dev formation T (°C)
1	–	Quartz 1.	11	308	38	–1.3	0.2	–	–
1	–	Quartz 2.	10	314	24	–1.3	0.2	–	–
1	–	Quartz 3.	5	70	8	–0.5	–	–	–
1	–	Chlorite	5	–	–	–	–	140	21
2–3	–	Quartz 1.	22	89	16	–0.6	–	–	–
2–3	–	Quartz 2.	10	103	24	–	–	–	–
4	type 1	Quartz 1.	8	295	22	–1.5	0.1	–	–
4	type 1	Quartz 2.	12	235	29	–1.4	0.2	–	–
4	type 1	Calcite	9	79	6	–0.5	0.1	–	–
4	type 1	Chlorite	5	–	–	–	–	209	14
5	type 1	Quartz 1.	14	289	37	–1.4	0.2	–	–
5	type 1	Quartz 2.	9	302	20	–1.6	0.1	–	–
5	type 1	Quartz 3.	6	74	6	–1.2	0.4	–	–
5	type 1	Chlorite	12	–	–	–	–	210	23
6	type 2	Quartz 2.	11	303	21	–0.6	0.2	–	–
6	type 2	Quartz 3.	2	152	–	–	–	–	–
6	type 2	Calcite	12	89	40	–0.8	0.5	–	–
8	type 2	Quartz 1.	13	233	38	–0.7	0.3	–	–
8	type 2	Quartz 2.	6	163	30	–0.6	0.3	–	–
8	type 2	Quartz 3.	4	111	2	–0.5	0.2	–	–
8	type 2	Calcite	14	81	13	–0.4	0.2	–	–
8	type 2	Chlorite 1.	3	–	–	–	–	259	16
8	type 2	Chlorite 2.	4	–	–	–	–	159	25
8	type 3	Quartz 1.	6	154	3	–	–	–	–
8	type 3	Chlorite	8	–	–	–	–	168	25
Total number of measurements:			221						

*: vein types according to GARUTI et al. 2011, applied only for samples, which were classified in that study.

impossible due to small crystal size and low transparency, therefore only a few data are available. Metastability often caused failure to observe the final melting temperatures, resulting in some cases incomplete data sets. Attempts to obtain measurements through heating were performed on sphalerite crystals, but due to its intensive cleavage upon heating above 150°C-200°C, no successful measurements were documented.

Results of the fluid inclusion microthermometry are presented in Table 2. and Fig. 5AB. In some cases, a high standard deviation was observed regarding Th, which may be interpreted as a result of temporal fluid evolution. This is proven by two facts. Firstly, in several cases, a Th increase of 10-15°C (at sites nr. 1 and 5) and Th decrease of 10-30°C (at sites nr. 4 and 8) were observed from the core to the rim of the same quartz crystal. Secondly, measurement of different sized inclusions in the same growth zone resulted in consistent Th values (maximum scattering was 7°C). This latter observation, in line with the experience of BODNAR (2003) (the smaller the size and higher the gas content characterising the inclusion, the higher the pressure that is needed to begin reequilibration), strengthens the lack of reequilibration processes.

Eutectic temperatures were determined in only a few cases, between -20.9°C and -22.4°C. Thus, NaCl-containing aqueous solution was applied for modelling the system. However, salinities were not calculated from the observed final melting temperature data (Table 2.), because the last solid to melt is CH_4 clathrate, as discussed in the following section. Due to the small size of the inclusions, it was generally only possible to observe the final melting, i.e. it was not possible to distinguish ice- and clathrate melting. A few available, uncertain data of ice melting scatter between $Tm_{(ice)}$=(-5.5)°C and (-5.9)°C, corresponding to a salinity of approx. 6.5 NaCl equiv. wt%.

6.4. Raman spectroscopy analyses

Raman spectroscopy analyses were carried out to examine the gas content and the accidentally trapped solid phases as well as to calculate salinity and the amount of gas in the quartz and calcite hosted primary fluid inclusions.

All the analysed accidentally trapped minerals were found to be sericite (muscovite). In the gas phase, the presence of methane was proven at sites nr. 1, 2-3, 4, 5, 6 and 8, in the primary inclusions of both quartz generations as well as in the calcite and no other gas phases were observed. The

Table 3: Salinity and methane content* of fluid inclusions based on the Raman spectroscopy analyses.

Site nr.	Vein type**	Mineral	Number of measurements	Average Th(LV-L) (°C)	St.dev. Th (°C)	Average salinity (NaCl equiv.wt%)	St.dev. salinity (NaCl equiv.wt%)	Average methane content (mol/kg)	St.dev. methane content (mol/kg)	Min/max minimum formation pressure (MPa)
1	–	Quartz 1.	5	295	19	9.00	0.62	–	–	–
2–3	–	Quartz 1.	4	88	7	10.49	0.57	–	–	–
5	type 1	Quartz 1.	5	250	14	10.19	1.20	–	–	–
8	type 2	Quartz 1.	6	202	18	8.06	1.45	0.28	0.06	31.2-38.5

*: the occurrence of methane was proven at sites nr. 1, 2-3, 4, 5, 6 and 8., but the exact methane content was calculated only where proper inclusions were found.
**: vein types according to GARUTI et al. 2011, applied only for samples, which were classified in that study.

Table 4: Selected chlorite analyses from the database of ZACCARINI and GARUTI (2008), representing the different vein types and localities.

			mass%											cation numbers (calculated for 14 O)													
Site nr.	Vein type*	mineral	SiO_2	TiO_2	Al_2O_3	Cr_2O_3	FeO	MnO	MgO	CaO	NaO	K_2O	Total	Si	Al (IV)	Al (VI)	Ti	Cr	Fe	Mn	Mg	Ca	K	Na	Total VI vacancy	XFe	T (°C) **
1	–	chlorite	30.88	0.00	12.72	0.00	14.78	0.62	22.37	0.31	0.05	0.04	82.04	3.30	0.70	0.91	0.00	0.00	1.32	0.06	3.57	0.04	0.01	0.01	5.90	0.10	0.27	162
4	type 1	chlorite	29.61	0.00	14.35	0.00	16.35	0.44	21.35	0.04	0.00	0.00	82.14	3.18	0.82	0.99	0.00	0.00	1.47	0.04	3.41	0.00	0.00	0.00	5.92	0.08	0.30	203
5	type 1	chlorite	31.86	0.01	17.05	0.04	11.02	0.28	25.05	0.33	0.03	0.01	85.68	3.16	0.84	1.15	0.00	0.00	0.91	0.02	3.70	0.04	0.00	0.01	5.84	0.16	0.20	208
8	type 2	chlorite 1.	30.70	0.00	17.71	0.06	17.48	0.54	23.13	0.24	0.02	0.01	89.87	3.01	0.99	1.06	0.00	0.00	1.43	0.04	3.39	0.02	0.00	0.00	5.96	0.04	0.29	255
8	type 2	chlorite 2.	30.71	0.02	12.24	0.01	19.54	0.40	18.10	0.41	0.08	0.01	81.53	3.38	0.62	0.96	0.00	0.00	1.80	0.04	2.97	0.05	0.00	0.02	5.84	0.16	0.37	139
8	type 3	chlorite	31.80	0.02	15.48	0.00	15.40	0.30	21.34	0.19	0.02	0.00	84.54	3.27	0.73	1.15	0.00	0.00	1.32	0.03	3.27	0.02	0.00	0.00	5.79	0.21	0.29	173

*: vein types according to GARUTI et al. 2011, applied only for samples, which were classified in that study
**: formation temperature calculation based on the method of CATHELINEAU & IZQUIERDO (1988)

occurrence of methane clathrate upon cooling was also confirmed (Fig. 6A, B, D).

Salinity calculations were performed based on the method of SUN et al. (2010), on fluid inclusions of randomly oriented quartz crystals from sites nr. 1, 2-3, 5. and 8. The calculated salinities are between 6.2 and 11.4 NaCl equiv. wt%, as presented in Table 3.

The amount of methane was calculated using the method of GUILLAUME et al. (2003), on fluid inclusions of Qtz1 from site nr. 8. This calculation is based on the Raman spectra of the homogenised liquid (Fig. 6C), measured only on large fluid inclusions in order to eliminate any expansion effect occurring during heating. The results of the calculations are presented in Table 3, together with the calculated homogenisation pressure (DUAN & MAO, 2006). Taking into consideration the homogenous nature of the parent fluid, this data corresponds to the minimum formation pressure.

6.5. Chlorite thermometry calculations

Chlorite analyses from the database of ZACCARINI & GARUTI (2008) were used to calculate the formation temperature of the chlorite crystals (see the representative analyses in Table 4.). Chlorite compositions measured in the same samples used for the fluid inclusion study to enable efficient comparison of the results. Instead of using the thermometry method of KRANIDIOTIS & MACLEAN (1987), suggested by ZACCARINI & GARUTI (2008), the method of CATHELINEAU & IZQUIERDO (1988) was used here, as the Al (IV) and XFe values of the measured data fitted into the criteria of the latter method. The calculated formation temperatures are $T_{formation}$=122-276°C, the details are shown in Table 2. and in Fig. 5C.

7. DISCUSSION

7.1. PTX conditions of the hydrothermal system

Several extensive studies and reviews have been published about submarine hydrothermal systems, summarising the

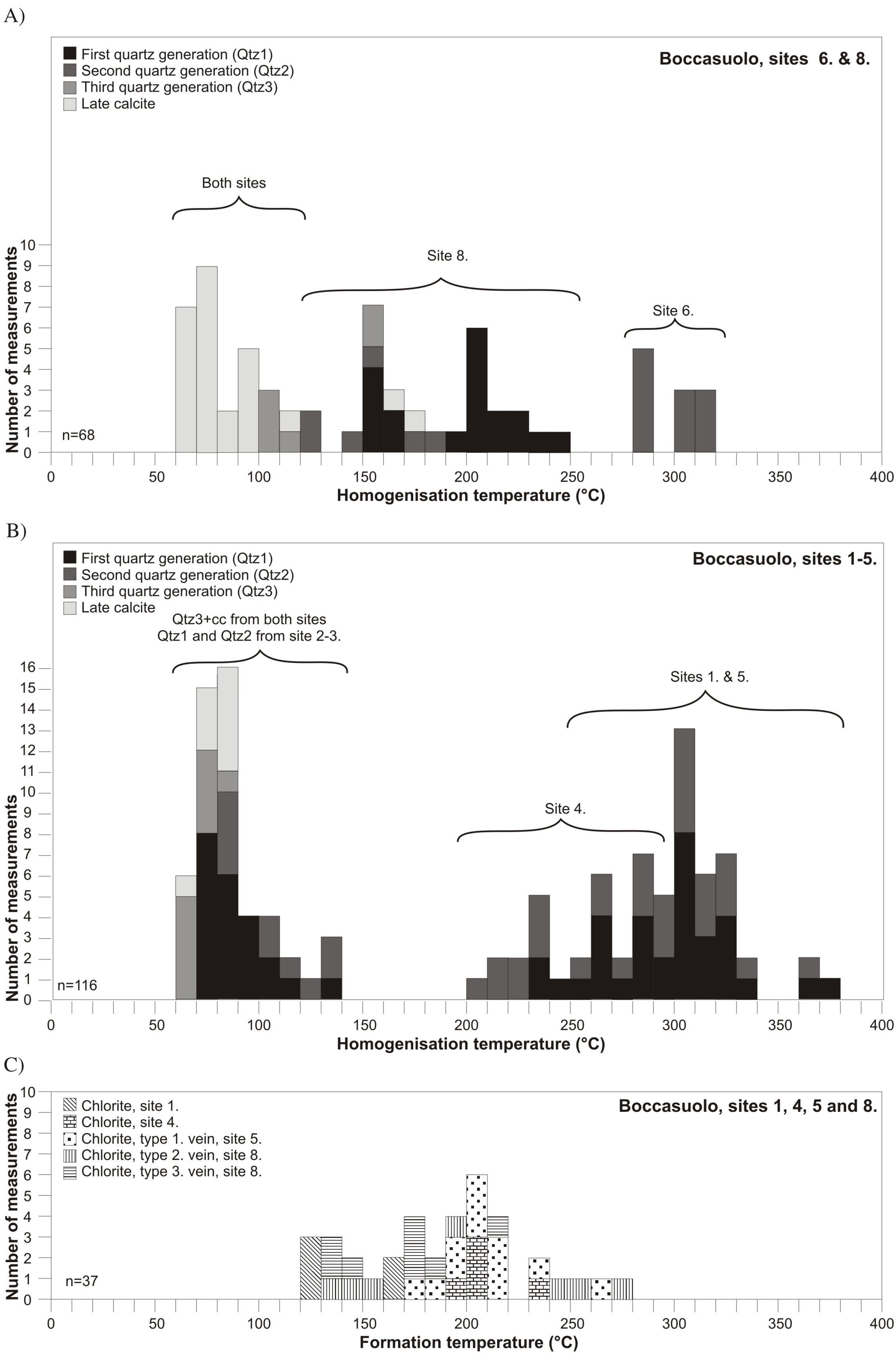

Figure 5: Minimum formation temperatures of quartz and calcite, as well as the formation temperature of chlorite at the different localities. **A:** A homogenisation temperature distribution diagram of quartz and calcite from the southern block of Boccassuolo (sites 6 and 8). **B:** Homogenisation temperature distribution diagram of quartz and calcite from the northern block of Boccassuolo (sites 1-5). **C:** Formation temperature of chlorite from different sites, based on chlorite thermometry calculations.

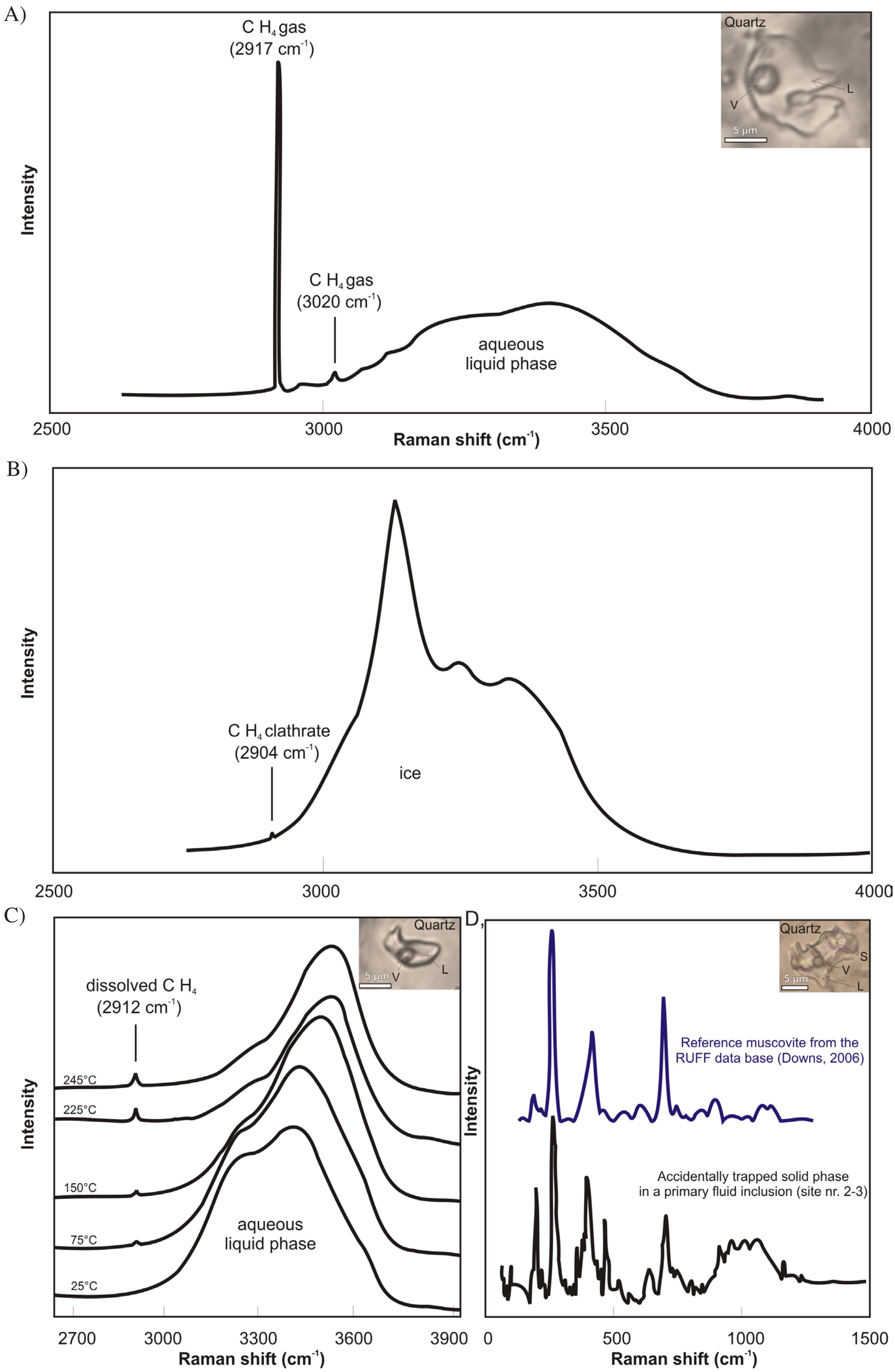

Figure 6: Results of the Raman spectroscopy analyses. **A:** Raman spectra of methane found in the gas phase of a primary fluid inclusion at lab temperature (25°C) (site nr. 8, Qtz1). **B:** Methane clathrate occurs together with ice, upon cooling, at -20°C (site nr. 1, Qtz1). **C:** Homogenisation experiment in a primary fluid inclusion. Upon heating, dissolved methane occurs in the liquid phase. Methane content calculations were performed at 20°C above the homogenisation temperature (245°C) (site nr. 8, Qtz1). **D:** Raman spectra of the accidentally trapped solid phase in a primary fluid inclusion at lab temperature (25°C). Background quartz was subtracted, in order to be able to identify muscovite. Reference muscovite from the RUFF data base (DOWNS, 2006) is also plotted (site nr. 2-3, Qtz1).

concepts on the sources, development and run of those processes (see e.g. RONA, 1984; HERZIG & HANNINGTON, 1995; WILKINSON, 2001; FOUSTOUKOS & SEYFRIED, 2007; PIRAJNO, 2009 and the references cited therein). Although many studies are available about both modern and ancient spreading ridge systems, significantly more results are published from other geodynamic environments (e.g. Kuroko-type systems, Iberian Pyrite Belt, Precambrian systems). WILKINSON (2001) and PIRAJNO (2009) agreed, however, that the concepts and knowledge about the Kuroko-type hydrothermal systems may be extended to other VMS deposits, therefore in the present discussion results and interpretations from different geodynamic environments are used.

7.2. Composition of the hydrothermal fluid

WILKINSON (2001) has reported a typical salinity range of 1-8.4 NaCl equiv. wt% for the hydrothermal fluids of the Kuroko-type deposits, similar to the 4±1.6 NaCl equiv. wt% result of NEHLIG (1991) from ophiolites and modern analogues. Other works have reported higher salinities up to 24 NaCl equiv. wt% in ancient VMS systems (e.g. China, ZENGQIAN et al., 2008, the Iberian Pyrite Belt, TORNOS, 2006). Moreover, the occurrence of even halite-bearing fluid inclusions were also documented both at Precambrian (salinities of 38.2 ± 1.9 NaCl equiv wt%, IOANNOU et al., 2007) and Phanerozoic locations (salinities up to 52 NaCl equiv. wt%, NEHLIG, 1991 and JUTEAU et al., 2000). A recent compilation by BODNAR et al. (2014) has confirmed a typical salinity range of 2-6 NaCl equiv. wt% for felsic, mafic and bimodal volcanism hosted VMS deposits, though higher salinity inclusions (99% of the data are within the range of 0-21 NaCl equiv. wt%) were also reported. Modification of the seawater may cause high salinity variations, the processes may involve fluid-rock interaction, mixing with seawater, phase separation (i.e., boiling), leaching of evaporites in the host sedimentary rocks, and/or mixing with magmatic volatiles, according to NEHLIG (1991), SCOTT (1997), WILKINSON (2001), FOUSTOUKOS & SEYFRIED (2007), PIRAJNO (2009), BODNAR et al. (2014) and references cited therein.

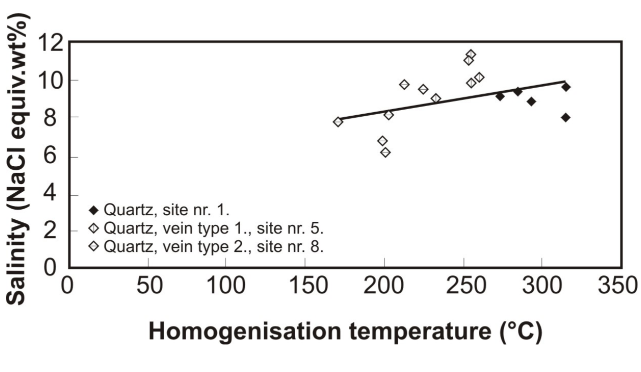

Figure 7: Homogenisation temperature (based on fluid inclusion microthermometry) vs. salinity (based on Raman spectroscopy) diagram of the quartz samples from Boccassuolo (data from the late fluid circulation event of site 2-3 are not presented).

In the case of Boccassuolo, the calculated (based on Raman spectra of the inclusions' fluid) salinities are between 6.2 and 11.4 NaCl equiv. wt% in the different vein types. Comparison of these data with the few available microthermometry based values (approx. 6.5 NaCl equiv. wt%), as well as cross-checks with other Raman spectra based methods (MERNAGH & WILDE, 1989) supports the validity of this latter approach, although the results still have to be handled with caution, knowing the uncertainties of the Raman spectra based salinity calculations (see e.g. BAUMGARTNER & BAKKER, 2009). The Th vs. salinity diagram shows a slight decrease of salinity with decreasing temperature (Fig. 7.), which can be explained by more intense mixing of hydrothermal fluids with seawater towards the top of the system.

The determined salinities indicate a modified seawater origin. As petrographic evidence of phase separation (coexisting liquid and vapour rich inclusions) was not observed, together with the fact that the Th vs. salinity diagram does not suggest mixing between two end-members, this process can be excluded as a possible source of seawater modification. Evaporites are not known in the host rock series. Therefore the two possible explanations would be the fluid-rock interaction and/or addition of magmatic volatiles. Similar salinity ranges were interpreted -with the help of O and H isotopes- as a result of modified seawater and magmatic fluid mixing at several Iberian Pyrite Belt localities (TORNOS, 2006), but simple fluid-rock interaction may also cause such elevated values (NEHLIG, 1991). Therefore both options could be reasonable explanations, and an unequivocal decision cannot be made based on the salinity values.

The presence of methane (average 0.28 mol/kg) may reveal further details. Though CO_2 is the most common volatile component in VMS systems (PIRAJNO, 2009), it was not observed in the studied fluid inclusions of Boccassuolo. Instead, a remarkable amount of methane occurred at both sites. Methane may form during biotic or abiotic (i.e., without involving organic matter) processes. CH_4 degassing (i.e. magmatic volatile) can be intense, if serpentinised peridotite is present, but methane can also occur in the system if seawater CO_2 is transformed to CH_4 after passing through the recharge zone, or it may occur as an indirect by-product of hydrothermal alteration of mafic rocks or graphitic, carbonaceous wall rocks (RONA, 1984, ZENGQIAN et al., 2008, PIRAJNO, 2009, ETIOPE & SCHOEL, 2014). In the studied area, interaction between the volcanic succession and sedimentary rocks is evidenced by the formation of corrensite (GARUTI et al., 2011). Additionally, serpentinised peridotite occurs also in the nearby ophiolites. Thus, an unequivocal decision cannot be made, a future detailed stable isotope study may help in answering this question.

The rather similar compositional features of the studied primary inclusions suggest that the different vein types (defined by GARUTI et al., 2011), all quartz generations and late calcite formed from the same evolved solution as part of the same hydrothermal process.

7.3. Pressure of the hydrothermal fluid

The typical water column in similar systems is 2.5 km in depth, which corresponds to a pressure of 25 MPa. In general, the depth of the stockwork zone is 100-300 m, up to 1-2 km below the seafloor, but typically remains within 1 km. Besides hydrostatic pressures, lithostatic or near-lithostatic pressures may also occur, if an independent and/or isolated convection cell forms at depth. Thus the characteristic pressure of the stringer zone is the sum of the hydrostatic pressure of the water column and the stringer zone and – if applicable – the lithostatic pressure. Generally it comprises 30-60 MPa, but in some cases, can reach 90 MPa, especially if self-sealing of the cracks is taken into consideration (e.g. SHERLOCK et al., 1999; IOANNOU et al., 2007; PIRAJNO, 2009; STEELE-MACINNIS, 2012 and references cited therein).

In Boccassuolo, the minimum formation pressure in the uppermost level of the deposit was 31.2-38.5 MPa. Considering that the total thickness of the pillow series did not exceed 500 m (PLESI et al., 2002), and calculating with a typical water column of 2.5 km, a total of 30-44 MPa pressure can be estimated. This approximation is in good agreement with the typical stockwork-zone pressures shown above, as well as with the observed minimum formation pressures. Hence no further pressure correction was performed on the obtained homogenisation temperature data.

7.4. Temperature of the hydrothermal fluid

In general, VMS stockwork mineralisations are interpreted as the discharge zone of the seafloor vents, formed at similar, or slightly higher temperatures, than the massive sulphide mound (e.g. ZENGQIAN et al., 2008 reported <220°C to >300°C in the stringer zone and 62-225°C in the massive sulphide body). A wider range of homogenisation temperatures (100-400°C) was also reported previously from different stringer zones (e.g. NEHLIG, 1991, PIRAJNO, 2009). BODNAR et al. (2014) also discovered that the homogenisation temperature from the VMS deposits are broadly consistent with the 'reaction zone" temperatures, reaching a maximum of less than ~400°C. The results obtained from Boccassuolo are in good agreement with the above mentioned facts, however, the measured homogenisation temperatures can be divided into three groups, indicating slightly different fluid evolution paths (Fig. 8).

The typical minimum formation temperatures at sites 1, 5 and 6 are 260-340°C. There the first two quartz generations are characterised by similar temperatures, thus a relatively consistent temperature environment can be concluded. The rather wide range can be the result of sampling from different parts of the same block, as within a single sample, the differences were always within 15°C.

The typical minimum formation temperatures at sites 4 and 8 are 150-290°C. There the first quartz generation yielded higher homogenisation temperatures than the second one. At these localities, relatively rapid cooling is concluded, emphasized by the observable temperature drop of 10-30°C within a single quartz crystal, from core to rim.

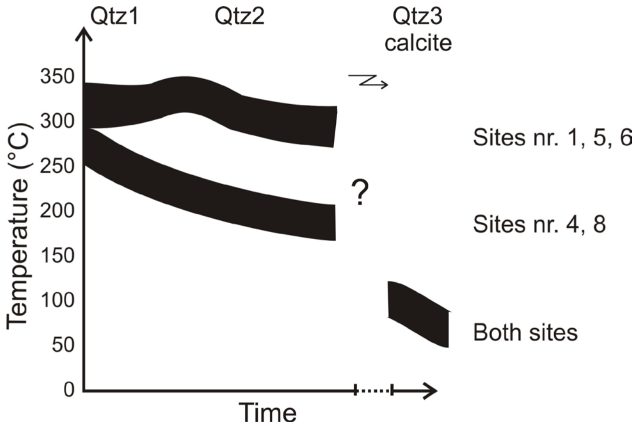

Figure 8: Schematic illustration of the typical fluid evolution paths (time vs. temperature) observed at sites 1, 4, 5, 6 and 8. Note, that relatively consistent temperature conditions were common at sites 1, 5 and 6, while a more rapid cooling was observed at sites 4 and 8. However, a later, low temperature event was common at every studied locality.

At both localities, a minimum formation temperature range of 60-130°C (generally in the third quartz generation and in calcite, but at sites 2, and 3 in each quartz generation) was also recorded. This can be interpreted as a low-temperature, later fluid circulation event, which belongs to the same, evolving hydrothermal process (see above).

In contrast to the fluid inclusion data, which are in good agreement with other VMS deposits, chlorite thermometry yielded slightly different results. ZACCARINI & GARUTI (2008) published a formation temperature range of 80-360°C for stockwork chlorites of the Northern Apennines VMS deposits, while in the case of Boccassuolo, only 122-276°C were observed (Fig. 5C). Both are in contrast with e.g. the Iberian Pyrite Belt results of 320-400°C by INVERNO et al. (2008). However, in the studied case, the thermometry results support the petrographic observations. It is proven that chlorite formed only rarely cogenetically with the highest temperature first quartz generation (see e.g. the results from site 8), but it precipitated mostly after or simultaneously with the second quartz generation (see e.g. the results from site 5). Thus it formed generally during the cooling of the system, filling the temperature gap between the high temperature quartz and the late fluid circulation event. Therefore, an additional step in the hydrothermal process is recognised with the help of this method. In contrast to the cautions against the use of this thermometer (see e.g. De CARITAT et al. 1993; JIANG et al. 1994; ESSENE & PEACOR, 1995), our observations confirm the use and validity of this method in the studied environment (similarly to the results reported by KISS et al., 2012, from a Hungarian Jurassic basaltic suite).

7.5. Spatial and temporal evolution of the hydrothermal system

7.5.1. Spatial distribution

The studied sites at Boccassuolo represent different levels of that ophiolitic sequence (611-874 m a.s.l.), although it is not necessary, that they were in a similar order upon their formation. While there is a known fault zone between sites 1-5 (northern block) and 6-8 (southern block), there is also the possibility of even smaller, so far unknown tectonic zones formed due to the obduction process (see also the dipping of the sequence). Therefore, the original structure of the stockwork zone is barely traceable and interpretation of the data according to the different sites is reasonable.

The observed ore and gangue minerals in the Boccassuolo VMS stockwork mineralisation (see e.g. the scarce occurrence of pyrrhotite and the common sericite, the latter also as an accidentally trapped solid phase in the fluid inclusions) have shown that the studied sites formed in distal locations, in relation to the centre of the fluid flow (see e.g. FRANKLIN et al. 1981; LYDON, 1984; HERZIG & HANNINGTON, 1995; BARRIE & HANNINGTON, 1999; PIRAJNO, 2009).

Numerical modelling of STEELE-MACINNIS et al. (2012) has revealed that the temperature along the stockwork zone is rather constant in the centre of the fluid flow, but decreases rapidly towards the distal parts. Thus significant vertical temperature zonation is not expected, but a horizontal one is presumed, explaining the presence of the three homogenisation temperature groups discussed above. Sites 1, 5 and 6, where no significant cooling was observed (Fig. 8.), were most probably located in the more central parts of the fluid flow, but still not in the core (see the slight temperature change and the sericite content). Sites 4 and 8, with more intense cooling (Fig. 8.), formed at a more distal location, while sites 2-3, where only low-temperature processes occurred, formed even farther away. This idea is also supported by the MgO content of the chlorite crystals: 21.75-27.20 wt% was observed at sites 1 and 5 (more central) and 14.86-24.64 wt% at sites 4 and 8 (more distal). According to URABE et al. (1983), higher concentration of MgO occurs in the alteration product chlorite close to the central parts of the system. Thus, the role of later tectonic movements is also indicated, bringing the more and less distal parts close to each other. However, the slightly lower temperatures and salinities observed in the southern block (caused by the more intense hydrothermal fluid-seawater mixing) reveal that this now higher altitude block was also originally located in a higher position in the sequence.

7.5.2. Temporal evolution

All the observations shown above reveal a temporal evolution in the hydrothermal system (Fig. 8.). Quartz formed in three successive generations, while chlorite formed cogenetically and epigenetically to quartz. Sphalerite most likely formed in the early stages of the hydrothermal activity, probably at a slightly lower temperature than the later chalcopyrite. Chalcopyrite formed probably at a slightly higher temperature, replacing the earlier minerals (see the slight Th increase in the more central sites from Qtz1 to Qtz2 (Fig. 8.), as well as within a single Qtz1 crystal). An excellent indicator for this process is the occurrence of chalcopyrite-disease in the early sphalerite, which is caused by replacement, with the reaction of the Fe-S content of the sphalerite with a later Cu-rich fluid (BARTON & BETHKE, 1987). A minor amount of sphalerite formed most probably during the waning of the system, together with late chalcopyrite (no chalcopyrite-disease is observable, but chalcopyrite inclusions in growth zones are found). Pyrite formed during the entire process, before, simultaneously and after the Cu and Zn-bearing minerals. A similar evolution was also observed by OHMOTO (1996) in Kuroko-type deposits.

However, a slightly different process took place in the central and the distal parts, depending mostly on how rapidly the formation temperature changed (Fig. 8.). This resulted in different ore mineral ratios (e.g. the amount of chalcopyrite is higher in the more central locations, and only pyrite occurs at the most distal one). This fact is proven by the chemical compositions of the veins (i.e. the occurrence of the different vein types 1, 2 and 3, defined by GARUTI et al. 2011); yielding up to 5.94 wt% Cu in samples from site 5 (originally more central location, type 1 vein) and up to 0.4 wt% Cu, but up to 1532 ppm Pb in samples from site 8 (originally more distal location, type 2 and 3 veins) (GARUTI et al., 2011). However, each locality suffered a late, low-temperature (<130°C) fluid circulation overprint, that still had similar characteristics (salinity, methane, sericite, fine-grained sulphide content), and can therefore be interpreted as a late result of the same hydrothermal process.

8. CONCLUSIONS

The detailed fluid inclusion, Raman spectroscopy and chlorite thermometry study of sulphide mineralised quartz veins of the Boccassuolo ophiolite helped to characterise the hydrothermal processes that occurred in this Jurassic VMS-related stockwork system. Besides rather common sulphide minerals (pyrite, chalcopyrite, sphalerite, pyrrhotite and galena), three quartz generations as well as chlorite, sericite and late carbonate were identified. The wide range of minimum formation temperatures (370-60°C) is most likely caused by the temporal evolution of the system as well as the more proximal vs. more distal position in relation to the centre of the hydrothermal fluid flow. Comparison of the minimum formation temperatures defined by the fluid inclusion study and the formation temperatures based on chlorite thermometry calculations (276-122°C) supported the petrographic observations; i.e. chlorite generally formed simultaneously and after the second quartz generation, within the temperature gap between the high temperature quartz and a late fluid circulation event. The salinity range (6.2-11.4 NaCl equiv. wt%) as well as the methane content (average 0.28 mol/kg) can both be explained by the formation of modified seawater, while petrographic observations and pressure estimations (30-44 MPa) suggest that boiling phenomena did not occur. Based on the fluid characteristics, the formation of the described vein types (1, 2, and 3) belongs to the same hydrothermal process. Modelling the temporal and spatial evolution of the system contributes significantly to our knowledge about the hydrothermal processes of the VMS systems of the N-Apennines, however, the results also illustrate the research efficiency and validity of the combination of fluid inclusion study, Raman spectroscopy and chlorite thermometry.

ACKNOWLEDGEMENT

Giorgio GARUTI and Federica ZACCARINI are thanked for providing the studied samples, for the information about the geological background, for the fruitful discussions and for the additional analysis of chlorite. The Research Instrument Core Facility (Eötvös Loránd University) and the Eugen F. STUMPFL Electron Microprobe Laboratory (University of Leoben) are thanked for the access to the Raman and EPMA laboratories, respectively. The research of G. B. KISS was supported by the European Union and the State of Hungary, co-financed by the European Social Fund in the framework of TÁMOP 4.2.4. A/1-11-1-2012-0001 'National Excellence Program'. Constructive comments of three reviewers were invaluable in helping to improve the original manuscript.

REFERENCES

ABBATE, E., BROTOLOTTI, V., PRINCIPI, G. (1980): Apennine ophiolites: a peculiar oceanic crust.– In: ROCCI, G. (ed.): Tethyan ophiolites. Ofioliti Spec. Issue, 1, 59–96.

BARRETT, T.J. (1982): Review of stratigraphic aspects of the ophiolite rocks and pelagic sediments of the Vara complex, North Apennines, Italy.– Ofioliti, 7/1, 3–46.

BARRETT, J.J. & FRIEDRICHSEN, H. (1989): Stable isotopic composition of atypical ophiolitic rocks from east Ligura, Italy.– Chem. Geol., 80, 71–84.

BARRETT, J.J. & SPOONER, E.F.C. (1977): Ophiolitic breccias associated with allochtonous oceanic crustal rocks in the Eastern Ligurian Apennines, Italy – A comparison with observations from rifted oceanic ridges.– Earth Planet. Sci. Letters, 35, 79–91.

BARRIE, C.T. & HANNINGTON, M.D. (1999): Introduction: Classification of VMS deposits based on host rock composition.– In: BARRIE, C.T. & HANNINGTON, M.D. (eds.): Volcanic-Associated Massive Sulfide Deposits: Processes and Examples in Modern and Ancient Settings. Rev. Econ. Geol., 8, 2–10.

BARTON, P.B. & BETHKE, P.M. (1987): Chalcopyrite disease in sphalerite: Pathology and epidemiology. Am. Mineral., 72, 451–467.

BAUMGARTNER, M. & BAKKER, R.J. (2009): Raman spectroscopy of pure H_2O and NaCl-H_2O containing synthetic fluid inclusions in quartz – a study of polarization effects. Miner. Petrol., 95, 1–15.

BERTOLANI, M. (1953): I giacimenti cupriferi dell'Appennino Modenese. Ricerche microscopiche a luce riflessa.– Atti Soc. Nat. Mat. Modena, 82, 3–10.

BODNAR, R.J. (2003): Reequilibration of fluid inclusions.– In: SAMSON, I., ANDERSON, A. & MARSHALL, D. (eds.): Fluid Inclusions: Analysis and Interpretation. Mineral. Assoc. Canada, Short Course, 32, 213–230.

BODNAR, R.J., LECUMBERRI-SANCHEZ, P., MONCADA, D. & STEELE-MACINNIS, M. (2014): Fluid Inclusions in Hydrothermal Ore Deposits.– In: HOLLAND, H.D. & TUREKIAN, K.K. (eds.): Treatise on Geochemistry, Second Edition, 13, 119–142. Oxford: Elsevier.

BONATTI, E., ZERBI, M., KAY, R. & RYDELL, H. (1976): Metalliferous deposits from the Apennine ophiolites: Mesozoic equivalents of modern deposits from oceanic spreading centres.– Bull. Geol. Soc. Am., 87, 83–94.

CABELLA, R., LUCCHETTI, G. & MARESCOTTI, P. (1998): Mn-ores from Eastern Ligurian ophiolitic sequences (»Diaspri di monte Alpe »formation, northern Apennines, Italy).– Trends Mineral., 2, 1–49.

CATHELINEAU, M. & IZQUIERDO, G. (1988): Temperature – composition relationships of authigenic micaceous minerals in the Los Azufres geothermal system.– Contrib. Mineral. Petrol., 100/4, 418–428.

CORTESOGNO, L., GIANNELLI, G. & PICCARDO, G.B. (1975): Petrogenesis and metamorphic evolution of the ophiolitic mafic rocks (Northern Apennine and Tuscany).– Boll. Soc. Geol. Ital., 94, 291–327.

CORTESOGNO, L., GALIBATI, B., PRINCIPI, G. & VENTURELLI, G. (1978): Le brecce ofiolitiche della Liguria orientale: nuovi dati e discussion sui modelli paleogeografici.– Ofioliti, 3, 99–160.

CORTESOGNO, L., GALBIATI, B. & PRINCIPI, G. (1987): Note alla „Carta geologica delle ofioliti del Bracco" e riconstruzione della paleogeografia Giurassico, Cretacica.– Ofioliti, 12, 261–342.

DAL PIAZ, G.V. (1974a): Le métamorphisme alpin de haute pression et basse temperature dans l'évolution structurale de bassin ophiolitique alpino-apeninique, 1e partie.– Boll. Soc. Geol. Ital., 93, 437–468.

DAL PIAZ, G.V. (1974b): Le métamorphisme alpin de haute pression et basse temperature dans l'évolution structurale de bassin ophiolitique alpino-apeninique, 2e partie.– Schweitzer Mineral. Petrol. Mitt., 57, 59–88.

DAOUDI, L. & POT DE VIN, J.-L. (2002): Thermal and hydrothermal effects of Triassic–Liassic basalt flow deposition on clays (Agana Basin, Morocco).– C.R. Geosci., 334/7, 463–468.

DE CARITAT, P., HUTCHEON, I. & WALSHE, J.L. (1993): Chlorite geothermometry: a review.– Clays Clay Miner., 41, 219–239.

DIAMOND, L.W. (2003): Systematics of H_2O inclusions.– In: SAMSON, I., ANDERSON, A. & MARSHALL, D. (eds.): Fluid Inclusions: Analysis and Interpretation. Mineral. Assoc. Can., Short Course Ser., 32, 55–79.

DILEK, Y. & FURNES, H. (2011): Ophiolite genesis and global tectonics: geochemical and tectonic fingerprinting of ancient oceanic lithosphere.– Bull. Geol. Soc. Am., 123, 387–411.

DILEK, Y. & FURNES, H. (2014): Ophiolites and their origins.– Elements, 10/2, 93–100.

DOWNS, R.T. (2006): The RRUFF Project: an integrated study of the chemistry, crystallography, Raman and infrared spectroscopy of minerals.– Program and Abstracts of the 19th General Meeting of the International Mineralogical Association in Kobe, Japan, O03-13.

DUAN, Z. & MAO, S. (2006): A thermodynamic model for calculating methane solubility, density and gas phase composition of methane-bearing aqueous fluids from 273 to 523 K and from 1 to 2000 bar.– Geochim. Cosmochim. Acta, 70, 3369–3386.

ELTER, P. (1975): L'ensemble ligure.– Bull. Soc. Geol. France, 17, 984–997.

ESSENE, E.J. & PEACOR, D.R. (1995): Clay Mineral Thermometry – A Critical Perspective.– Clays Clay Miner., 43, 540–553.

ETIOPE, G. & SCHOEL, M. (2014): Abiotic gas: atypical, but not rare.– Elements, 10/4, 291–296.

FERRARIO, A. & GARUTI, G. (1980): Copper deposits in the basal breccias and volcanosedimentary sequences of the Eastern Ligurian ophiolites (Italy). Mineral. Dep., 15, 291–303.

FOUSTOUKOS, D.I. & SEYFRIED, W.E. (2007): Fluid phase separation processes in submarine hydrothermal systems. Rev. Mineral. Geochem., 65, 213–239.

FRANKLIN, J. M., SANGSTER, D.,M. & LYDON, J.,W. (1981): Volcanic Associated Massive Sulphide Deposits. Econ. Geol. 75th Anniversary Vol., 485–627.

GARUTI, G. & ZACCARINI, F. (2005): Minerals of Au, Ag and U in volcanic-rock-associated massive sulphide deposits of the Northern Apennine ophiolite, Italy.– Can. Mineral., 43, 935–950.

GARUTI, G., BARTOLI, O., SCACCHETTI, M. & ZACCARINI, F. (2008): Geological setting and structural styles of Volcanic Massive Sulphide deposits in the Northern Apennines (Italy): evidence for seafloor and sub-seafloor hydrothermal activity in unconventional ophiolites of the Mesozoic Tethys. Bol. Soc. Geol. Mex., 60/1, 121–145.

GARUTI, G. ALFONSO, P., ZACCARINI, F. & PROENZA, J.A. (2009): Sulfur-isotope variations in sulphide minerals from massive sulphide deposits of the Northern Apennine ophiolites: inorganic and biogenic constraints. Ofioliti, 34, 43–62.

GARUTI, G., ZACCARINI, F., SCACCHETTI, M. & BARTOLI, O. (2011): The Pb-rich sulphide veins in the Boccassuolo ophiolite: Implications for the evolution of hydrothermal activity accross the ocean-continent transition in the Ligurian Tethys (Northern-Apennine, Italy). Lithos, 124, 243–254.

GOLDSTEIN, R. H. & REYNOLDS, T. J. (1994): Systematics of fluid inclusions in diagenetic minerals. Soc. Sedim. Geol. Short Course, 31, 199 p.

GUILLAUME, D., TEINTURIER, S., DUBESSY, J. & PIRONON J. (2003): Calibration of methane analysis by Raman spectroscopy in H_2O–NaCl–CH_4 fluid inclusions. Chem. Geol., 194, 41–49.

HERZIG, P.M. & HANNINGTON, M.D. (1995): Polymetallic massive sulphides at the modern seafloor: A review.– Ore Geol. Rev., 10, 95–115.

INVERNO, C.M.C., SOLOMON, M., BARTON, M.D. & FODEN, J. (2008): The Cu stockwork and massive sulfide ore of the Feiteis volcanic-hosted massive sulfide deposit, Aljustrel, Iberian Pyrite Belt, Portugal: A mineralogical, fluid inclusion, and isotopic investigation.– Econ. Geol., 103, 241–267.

IOANNOU, S.E., SPOONER, E.T.C. & BARRIE, C.T. (2007): Fluid Temperature and Salinity Characteristics of the Matagami Volcanogenic Massive Sulphide District, Quebec. Econ. Geol., 102, 691–715.

JIANG, W.T., PEACOR, D.R. & BUSECK, P.R. (1994): Chlorite Geothermometry? – Contamination and Apparent Octahedral Vacancies.– Clays Clay Miner., 42, 593–605.

JUTEAU, T., MANAC'H, G., MOREAU, O., LÉCUYER, C. & RAMBOZ, C. (2000): The high temperature reaction zone of the Oman ophiolite: new field data, microthermometry of fluid inclusions, PIXE analyses and oxygen isotopic ratios.– Mar. Geophys. Res., 21/3, 351–385.

KISS, G., MOLNÁR, F. & ZACCARINI, F. (2012): Fluid inclusion studies in datolite of low grade metamorphic origin from a Jurassic pillow basalt series in northeastern Hungary.– Central Eur. J. Geosci., 4/2, 261–274.

KRANIDIOTIS, P. & MACLEAN, W.H. (1987), Systematics of chlorite alteration at the Phelps Dodge massive sulphide deposit, Matagami, Quebec.– Econ. Geol., 82., 1898–1911.

LAGABRIELLE, Y. & LEMOINE, M. (1997): Alpine, Corsican and Apennine ophiolites: the slow-spreading ridge model.– C. R. Acad. Sci. Paris, 325, 909–920.

LEMOINE, M., TRICART, P. & BOILLOT, G. (1987): Ultramafic and gabbroic ocean floor of the Ligurian Tethys (Alps, Corsica, Apennines): in search of a genetic model. Geology, 15, 622–625.

LEONI, L., SARTORI, F. & TAMPONI, M. (1998), Compositional variation in K-micas and chlorites coexistiong in Al-saturated metapelites under late-diagenetic to low-grade metamorphic conditions (Internal Liguride Units, Northern-Apennines, Italy).– Eur. J. Mineral., 10, 1321–1339.

LOMBARDO, B., RUBATTO, D. & CASTELLI, D. (2002): Ion microprobe U-Pb dating of zircon from a Monviso metaplagiogranite: implication for the evolution of the Piedmont-Liguria Tethys in the Western Alps.– Ofioliti, 27/2, 119–131.

LYDON, J. W. (1984): Some observations on the morphology and ore textures of volcanogenic sulfide deposits of Cyprus. Geol. Surv. Canada, Curr. Res., Paper 84-01A, 601–610.

MERNAGH, T.P. & WILDE, A.R. (1989): The use of the laser Raman microprobe for the determination of salinity in fluid inclusions. Geochim. Cosmochim. Acta, 53/4, 765–771.

NEHLIG, P. (1991): Salinity of oceanic hydrothermal fluids: a fluid inclusion study. Earth Planet. Sci. Letters, 102, 310–325.

OHMOTO, H. (1996): Formation of volcanogenic massive sulphide deposits: the Kuroko perspective. Ore Geol. Rev., 10, 135–177.

PICCARDO, G.B., RAMPONE, E. & ROMAIRONE, A. (2002): Formation and composition of the oceanic lithosphere of the Ligurian Tethys: inferences from the Ligurian ophiolites. Ofioliti, 27/2, 145–161.

PINI, G.A. (1999): Tectonosomes and olistostromes in the Argille Scagliose of the Northern Apennines, Italy. Geol. Soc. Am. Spec. Pap., 335, 1–70.

PIRAJNO, F. (2009): Hydrothermal processes and mineral systems: Springer, Geological Survey of Western Australia, 1250 p.

PLESI, G., DANIELE, G., CHICCI, S., BETTELLI, G., CATANZARITI, R., FERONI, C., De NARDO, M.T., MARTINELLI, P., OTTRIA, G. & PANINI, F. (2002): Note illustrative della Carta Geologica d'Italia alla scala 1:50.000, foglio 235 Pievepelago : Presidenza del Consiglio dei Ministri, Servizio Geologico d'Italia, Regione Emilia Romagna, 1–138.

POGNANTE, U. & PICCARDO, G.B., (1984): Petrogenesi delle ofioliti delle Alpi Occidentali.– Mem. Soc. Geol. Ital., 29, 79–92.

PRINCIPI, G., CORTESOGNO, L., CELLAI, D., GAGGERO, L., GARUTI, G., GAZZOTTI, M., PASSERINI, P. & TREVES, B. (1992): Le ofioliti dell'Apennino settentrionale : Societá Geologica Italiana, 76a Riunione Estiva, Firenze 24-25-26 settembre 1992, Guide alle Escursioni post-congresso, 1–76.

RONA, P.A. (1984): Hydrothermal mineralization at seafloor spreading centres.– Earth Sci. Rev., 20, 1–104.

SCOTT, S.D. (1997): Submarine hydrothermal systems and deposits: In Barnes, H.L. (ed.): Geochemistry of hydrothermal ore deposits, 3rd ed.: New York, John Wiley and Sons, 797–875.

SHERLOCK, R.L., ROTH, T., SPOONER, E.T.C. & BRAY, C.J. (1999): Origin of the Eskay Creek Precious Metal-Rich Volcanogenie Massive Sulphide Deposit: Fluid Inclusion and Stable Isotope Evidence.– Econ. Geol., 94, 803-824.

STEELE-MACINNIS, M., HAN, L., LOWELL, R.P., RIMSTIDT, J.D. & BODNAR R.J. (2012): Quartz precipitation and fluid inclusion characteristics in sub-seafloor hydrothermal systems associated with volcanogenic massive sulphide deposits.– Centr. Eur. J. Geosci., 4/2, 275–286.

SUN, Q., ZHAO, L., LI, N. & LIU, J. (2010): Raman spectroscopic study for the determination of Cl− concentration (molarity scale) in aqueous solutions: Application to fluid inclusions.– Chem. Geol., 272, 55–61.

TORNOS, F. (2006): Environment of formation and styles of volcanogenic massive sulphides: the Iberian Pyrite Belt.– Ore Geol. Rev., 28, 259–307.

URABE, T., SCOTT, S.D. & HATTORI, K. (1983): A comparison of footwall-rock interactions and geothermal systems beneath some Japanese and Canadian volcanogenic massive sulphide deposits.– Econ. Geol. Monograph, 5, 345–364.

WILKINSON, J.J. (2001): Fluid inclusions in hydrothermal ore deposits.– Lithos, 55, 229–272.

ZACCARINI, F. & GARUTI, G. (2008): Mineralogy and chemical composition of VMS deposits of northern Apennine ophiolites, Italy: evidence for the influence of country rock type on ore composition.– Mineral. Petrol., 94, 61–83.

ZACCARINI, F., MORALES-RUANO, S., SCACCHETTI, M. & GARUTI, G. (2008): Investigation of datolite ($CaBSiO_4OH$) from basalts in the northern Apennines ophiolites (Italy): genetic implications. Chemie Erde – Geochem., 86, 265–277.

ZENGQIAN, H., ZAW, K., RONA, P., LINQUING, L., XIAOMING, Q., SHUHE, S., LIGUI, P. & JIANJUN, H. (2008): Geology, Fluid Inclusions, and Oxygen Isotope Geochemistry of the Baiyinchang Pipe-Style Volcanic-Hosted Massive Sulphide Cu Deposit in Gansu Province, Northwestern China.– Econ. Geol., 103, 269–292.

Manuscript received January 26, 2015
Revised manuscript accepted September 05, 2015
Available online October 31, 2015